# Anthropogenic Iron Deposition Alters the Ecosystem and Carbon Balance of the Indian Ocean Over a Centennial Timescale

Anh Le-Duy Pham, Takamitsu Ito

JGR Oceans

RESEARCH ARTICLE
10.1029/2020JC016475

**Key Points:**

- Ecosystem dynamics controls the centennial response of the Indian Ocean carbon cycling to anthropogenic nutrients depositions
- The competition between phytoplankton community leads to opposite responses of the ocean carbon uptake in different regions
- Iron distribution biases in previous modeling studies can underestimate the response of the ocean ecosystem

**Supporting Information:**

- Supporting Information S1

**Correspondence to:**
A. L. D. Pham,
anhlpham@gatech.edu

**Citation:**
Pham, A. L. D., & Ito, T. (2021). Anthropogenic iron deposition alters the ecosystem and carbon balance of the Indian Ocean over a centennial timescale. *Journal of Geophysical Research: Oceans*, *126*. e2020JC016475. https://doi.org/10.1029/2020JC016475

Received 3 JUN 2020
Accepted 27 JAN 2021



# Anthropogenic Iron Deposition Alters the Ecosystem and Carbon Balance of the Indian Ocean Over a Centennial Timescale

**Anh L. D. Pham[1,2] and Takamitsu Ito[1]**

[1]School of Earth and Atmospheric Sciences, Georgia Institute of Technology, Atlanta, GA, USA, [2]Now at Laboratoire d'Océanographie et de Climatologie: Expérimentation et Approches Numériques (LOCEAN), IPSL, CNRS/UPMC/IRD/MNHN, Paris, France

**Abstract** Phytoplankton growth in the Indian Ocean is generally limited by macronutrients (nitrogen: N and phosphorus: P) in the north and by micronutrient (iron: Fe) in the south. Increasing atmospheric deposition of N and dissolved Fe (dFe) into the ocean due to human activities can thus lead to significant responses from both the northern and southern Indian Ocean ecosystems. Previous modeling studies investigated the impacts of anthropogenic nutrient deposition on the ocean, but their results are uncertain due to incomplete representations of the Fe cycling. This study uses a state-of-the-art ocean ecosystem and Fe cycling model to evaluate the transient responses of ocean productivity and carbon uptake in the Indian Ocean, focusing on the centennial time scale. The model includes three major dFe sources and represents an internal Fe cycling modulated by scavenging, desorption, and complexation with multiple, spatially varying ligand classes. Sensitivity simulations show that after a century of anthropogenic deposition, ecosystem responses in the Indian Ocean are not uniform due to a competition between the phytoplankton community. In particular, the competition between diatom, coccolithophore, and picoplankton alters the balance between the organic and carbonate pumps in the Indian Ocean, increasing the carbon uptake along 50°S and the southeastern tropics while decreasing it in the Arabian Sea. Our results reveal the important role of ecosystem dynamics in controlling the sensitivity of carbon fluxes in the Indian Ocean under the impact of anthropogenic nutrient deposition over a centennial timescale.

**Plain Language Summary** Human activities have intensified the atmospheric nutrient input into the Indian Ocean where the marine ecosystem is diverse and biogeochemical features are complex. Thus, the response of the marine ecosystem in this region to human perturbations can be significant. Results from previous studies on this topic are uncertain due to our limited understanding of the ocean micronutrient, iron. In this study, we address this issue through a suite of computer simulations with an improved iron cycling model. We found that after a century of anthropogenic deposition, the ocean carbon uptake is enhanced in the southeastern tropics of the Indian Ocean. However, the carbon uptake decreases in the Arabian Sea because the ecosystem shifts toward organisms that produce calcite, which changes the ocean chemistry and weakens its ability to absorb carbon dioxide.

## 1. Introduction

The Indian Ocean accounts for around one-fifth of the ocean net primary production (Behrenfeld & Falkowski, 1997a) and contains two of the largest oxygen ($O_2$) minimum zones (OMZs) of the world oceans in the northern part (the Arabian Sea and the Bay of Bengal) (Stramma et al., 2010). In these two regions, phytoplankton growth is generally limited by macronutrients because of the relatively shallow mixed layer and the Ekman downwelling that transports nutrients away from the euphotic layer. Furthermore, the low $O_2$ water in the OMZs promote nitrogen (N) loss through denitrification (Moore et al., 2013; Wang et al., 2019). In the northern Indian Ocean, the concentration of dissolved iron (dFe) is relatively high (~0.6 nM in the surface and ~1.5 nM in the subsurface 200–1,000 m water) due to relatively high dFe inputs from atmospheric deposition and reduced sediments over the continental shelves (Chinni et al., 2019; Nishioka et al., 2013). However, Fe can still be a limiting factor for the nitrogen-fixer diazotrophs, which have a higher demand for Fe than other phytoplankton (Moffett et al., 2015; Moore et al., 2013). In contrast,

the southern part of the Indian Ocean shows a very low dFe concentration (~0.2 nM), indicating that the biological productivity in this region can be Fe-limited (Chinni et al., 2019; Nishioka et al., 2013). These contrasting biogeochemical regimes between different parts of the Indian Ocean imply a diverse and complex response of the marine ecosystem to perturbations. While recent observations showed that the Indian Ocean phytoplankton community has changed due to environmental variations, mechanisms controlling these changes are not well understood (Mishra et al., 2015; Naik et al., 2020; Roxy et al., 2016; Tripathy et al., 2020).

Atmospheric deposition of N and dFe into the Indian Ocean has been increasing due to human activities, which including burning of fossil fuels, agriculture, and land use changes (Baker et al., 2017; Duce et al., 2008; Mahowald et al., 2009). Human activities also emit anthropogenic aerosols, which modify mobilization processes and atmospheric processing. Atmospheric dust deposition, which is generally stronger in the northern Indian Ocean, provides a direct input of bioavailable N, potentially relieving the macronutrient limitation. Increased atmospheric deposition can also provide dFe to support the growth of diazotrophs, and the deposited dFe can be transported to the southern part of the Indian Ocean (Boyd & Tagliabue, 2015). In general, a significant response of the Indian Ocean ecosystem to anthropogenic deposition from the atmosphere is expected, possibly including a higher organic carbon export flux, stronger $O_2$ demand, thus an increase of the ocean carbon uptake and an expansion of OMZs (Moffett et al., 2015).

Recent modeling studies have examined the impact of anthropogenic nutrient deposition into the ocean by driving ocean biogeochemistry models with atmospheric deposition fields derived from atmospheric chemical transport models (Guieu et al., 2019; Ito et al., 2016; Krishnamurthy et al., 2007, 2009). These studies concluded that increasing dFe and N inputs stimulate marine nitrogen fixation in the subtropical North and South Pacific, enhance the primary production and export in the high-nutrient low-chlorophyll (HNLC) regions (Krishnamurthy et al., 2009), and accelerate the $O_2$ consumption in the tropical Pacific Ocean (Ito et al., 2016). Concurrently, the data coverage of dFe and other trace metal species expanded significantly thanks to the GEOTRACES program (Mawji et al., 2015; Schlitzer et al., 2018). The new observations revealed shortcomings of the earlier generations of the Fe cycling models, which did not include all of the dFe sources such as hydrothermal vents. Also, earlier models typically assumed a single ligand class with a uniform distribution. Thus, results from these earlier studies can contain significant uncertainty (Tagliabue et al., 2016). Significant model biases have been identified relative to the observed pattern of dFe revealed by the recent GEOTRACES observations (Mawji et al., 2015; Schlitzer et al., 2018). Models with constant ligand concentrations may underestimate the feedback between biological activity, ligand production, and dFe concentration to environmental changes (Völker & Tagliabue, 2015). Furthermore, impacts of anthropogenic atmospheric deposition on the Indian Ocean, where the nutrient cycling is complex and the phytoplankton community is diverse, has not been examined thoroughly and systematically.

This study aims to investigate the impact of increasing anthropogenic atmospheric N and dFe deposition on nutrient distribution, phytoplankton productivity, and the ocean carbon uptake in the Indian Ocean. We focus on the response of the ocean ecosystem over a timescale of 100 years, which is relevant to human activities and policy decisions. To this end, we use a 3-D global ocean ecosystem model (MITgcm), which represents major phytoplankton types (Dutkiewicz et al., 2014), coupled with a recently improved Fe cycling scheme (Pham & Ito, 2018, 2019). The Fe scheme includes many crucial processes controlling ocean Fe cycling and demonstrated improvements in the representation of dFe distribution as observed by the GEOTRACES cruises. The ecosystem fields of the model have been systematically evaluated against available observations (Dutkiewicz et al., 2009, 2012). This ecosystem model has also been used in many previous studies to evaluate the ocean biogeochemistry response to human perturbations (Dutkiewicz et al., 2013, 2014) and the interplay between different bigeochemical processes shaping the phytoplankton community structure (Dutkiewicz et al., 2012). While we acknowledge the low resolution of this model and its potential biases, this model allows us to perform a suite of sensitivity simulations to test different hypotheses without a high computational cost. Atmospheric deposition of dFe and N are derived from the 3-D atmospheric chemical transport model GEOS-Chem coupled with a comprehensive dust-Fe dissolution scheme (Ito et al., 2016; Johnson & Meskhidze, 2013). The rest of the study is organized as follows. In Section 2, we describe the model configuration and the experimental design. In Section 3, we present results of sensitivity experiments. In Section 4, we summarize the results and discuss their implications.

## 2. Model Configuration and Experimental Design

The global ocean model used in this study was based on the Massachusetts Institute of Technology general circulation model (Marshall, Adcroft, et al., 1997; Marshall, Hill, et al., 1997, MITgcm) with a biogeochemistry and ecosystem component (Dutkiewicz et al., 2012, 2014). The model domain was configured for a 2.8° × 2.8°horizontal grid spacing, and 23 vertical z-levels with grid spacing ranging from 10 m in the surface to 500 m at 5,000 m. Ocean boundary layer physics was parameterized using the K-Profile Parameterization scheme (Large et al., 1994), and the effects of mesoscale eddies was parameterized using the isopycnal tracer and thickness diffusion scheme (Gent & Mcwilliams, 1990). The physical ocean circulation was forced by climatological wind and buoyancy forcing derived from the National Center for Environmental Prediction Reanalysis product (Kalnay et al., 1996).

The biogeochemical component of the model was based on Dutkiewicz et al. (2014), including the cycling of carbon (C), P, N, silica (Si), Fe and $O_2$ through inorganic, living, dissolved, and particulate organic phases. Two grazers and six phytoplankton types (diatom, coccolithophore, large eukaryotes, *Prochlorococcus*, other picophytoplankton, and diazotrophs) were represented in the model. The phytoplankton growth rate was a function of the Chlorophyll: C ratio, temperature, light, and nutrient availability, following Hickman et al. (2010) and Geider et al. (1998).

The refined Fe scheme, which were developed and documented in our recent publications (Pham & Ito, 2018, 2019), encompassed various important processes in the ocean Fe cycling. These processes included external dFe inputs from dust deposition, continental shelves, and hydrothermal vents. The model's internal cycling of Fe considered scavenging of dFe onto and release of dFe from organic and lithogenic particles and dFe retention by spatially varying organic ligands. Scavenging of free dFe (Fe'), which is not bound to ligands, by organic particles was parameterized as a function of the concentrations of particulate organic matter and of Fe'. dFe scavenged by this process can be released back to the water column through the remineralization of sinking organic particles (reversible scavenging) (Boyd et al., 2010). Different from the model used in previous publications (Pham & Ito, 2018, 2019), particulate organic matter is a prognostic variable in this model, and therefore its vertical attenuation with depth was explicitly calculated. As in Pham and Ito (2018, 2019), the inorganic scavenging process was parameterized as a first order loss process with a rate constant, $k_{\mathrm{inorg}}$. This rate constant can significantly increase under the dust plume where elevated dust deposition increases the lithogenic particle concentration (Ye & Völker, 2017). This mechanism was represented in the model by scaling $k_{\mathrm{inorg}}$ with the atmospheric dFe flux. Scavenged dFe through this mechanism can also return to the water column by desorption from sinking particles. This return dFe flux was calculated from the vertical profile of sinking inorganic scavenged-Fe flux, which was represented by a power function with a coefficient of −0.4 (Pham & Ito, 2019). Atmospheric deposition fields of N and dFe were taken from the output of atmospheric chemical transport model GEOS-Chem (Johnson & Meskhidze, 2013). Anthropogenic effects on N and dFe deposition were calculated using the emission inventories for the year 2009, and the preindustrial fluxes were calculated by turning off all anthropogenic emission sources. Details on this model and how the industrial fluxes were calculated based on anthropogenic emission were described in Ito et al. (2016) and Johnson and Meskhidze (2013).

The model was first spun up under the preindustrial deposition of N and dFe for 1,000 years (*PreIn* run). Initialized from the last time step of the *PreIn* run, a suite of additional integrations was performed using the anthropogenic deposition of N and dFe. These simulations were further integrated for 1,000 years to achieve new quasisteady states. Results of the final year of the 1,000-year model run forced under the anthropogenic deposition were used to evaluate the performance of different model runs against available observations (temperature, salinity, $PO_4^{3-}$, $NO_3-$, dFe, and net primary production [NPP]). However, we only analyzed the response of the ecosystem and carbon cycle to the anthropogenic deposition during the first 100 years. These experiments intended to examine the centennial impacts of anthropogenic N and dFe deposition on the Indian Ocean. In addition, we aimed to evaluate how recent improvements in our model representation of the ocean Fe cycling alter the responses of the ocean ecosystem. Thus, we performed two more model experiments where the ocean Fe cycling has a simpler representation (a uniform, constant ligand class and an irreversible scavenging scheme), which was used in previous modeling studies. In reality, there could be transient perturbations to the marine ecosystem and biogeochemistry on all timescales, including the effects of warming and increased stratification, circulation changes, riverine nutrient input, and acidification.

Accounting for all these changes is beyond the scope of this paper. As a first step, we focused on a single perturbation in the atmospheric nutrient deposition to better understand the response to this particular anthropogenic forcing. In summary, model experiments were set up as follows:

- "*PreIn*" run forced by the preindustrial atmospheric dFe and N deposition fields
- "*Ind*" run forced by the contemporary atmospheric dFe and N deposition fields
- "*IndN*" run forced by the contemporary atmospheric N deposition field and preindustrial dFe
- "*IndFe*" run forced by the contemporary atmospheric dFe field and preindustrial N
- "*SimpleFe-PI*" run forced by the same forcing as the *PreIn* run but has a simpler Fe cycling scheme: constant concentration of ligand (1 nM) and an irreversible scavenging removal for Fe
- "*SimpleFe*" run forced by the same forcing as the *Ind* run but has a simpler Fe cycling scheme

Results from the sensitivity runs were analyzed by comparing the differences in nutrient fields, biological productivity, phytoplankton community structure, and carbon uptake, all in relation to the *PreIn* run. The exception is for the *SimpleFe* run, where results from this run were compared with *SimpleFe-PI* run.

## 3. Results

### 3.1. Model Validation

We first evaluated the model performance and its ability to reproduce major biogeochemical features of the Indian Ocean by comparing the observed, modern distributions of nutrient tracers with the equilibrium state of the *Ind* model run, which is forced by contemporary forcings.

Biological productivity is influenced by the nutrient distributions, thus it is essential that the model captures the nutrient fields well. First, we examined the model nitrate ($NO_3^-$) distribution using the World Ocean Atlas (Garcia et al., 2014) as the observational benchmark (Figure 1a). The model is certainly not perfect as it underestimated the $NO_3-$ concentrations at high latitudes and overestimated $NO_3-$ in the equatorial region. However, the general pattern of the near-surface $NO_3-$ distribution was captured reasonably well (Figure 1b). When compared to the World Ocean Atlas, the model reproduced the boundary between the low and high concentration approximately at 40°S.

Next, we examined the meridional transect of dFe along the GEOTRACES line GI04 (Schlitzer et al., 2018), but focusing on the upper ocean (0–1,000 m) since the upper dFe distribution is more important for sustaining biological productivity. GEOTRACES is an international study which combines ocean sections, process studies, data synthesis, and modeling to identify and quantify the processes regulate trace elements and their isotopes within and between ocean basins (Schlitzer et al., 2018). Recent observational data from the GEOTRACES GI04 transect provided a large-scale, basin-scale full-depth section profile of dFe in the Indian Ocean, from the Arabian Sea to the Southern Ocean (Nishioka et al., 2013). The model captured the pattern of dFe remarkably well especially in the top 1,000 m, consistent with results shown by Pham and Ito (2018) (Figures 1d and 1e). Specifically, it captured the strong meridional gradient of dFe centered at around 10°S where the observed dFe concentration is high (0.8–1.3 nM) in the subsurface water of the tropical thermocline but it is very low in the south of 20°S (~0.2 nM). The model also reproduced the subsurface peak of dFe in the northern Arabian Sea (~10°N) and the strong vertical gradient in the dFe concentration observed there between the surface (0–200 m) and subsurface waters (>200 m). The only major bias in this model is the underestimation of hydrothermal signal around the Central Indian Ridge segment 3,000 m depth between 30°S and 5°N. This is likely because our model did not represent the unique interaction between particulate and dissolved phases of Fe released from the vents, which supports the lateral transport of dFe away from the vent sources (Fitzsimmons et al., 2017). Moreover, measurements by Fitzsimmons et al. (2017) show that a large portion of dFe released from hydrothermal vents can be nanoparticles of pyrite or Fe(III) oxides, which are not represented in the model.

When compared with the zonal mean of the satellite-derived annual mean NPP averaged from 2003 to 2016 (Behrenfeld & Falkowski, 1997b) in the Indian Ocean (Figure S1), our model showed an underestimation for NPP in the subtropics and in the southern Indian Ocean (south of ~20°S). This is a common deficiency of coarse-resolution ocean ecosystem models (Dutkiewicz et al., 2012, 2013, 2014), which do not adequately represent the coastal current systems and open ocean eddies. Without these small-scale processes, the

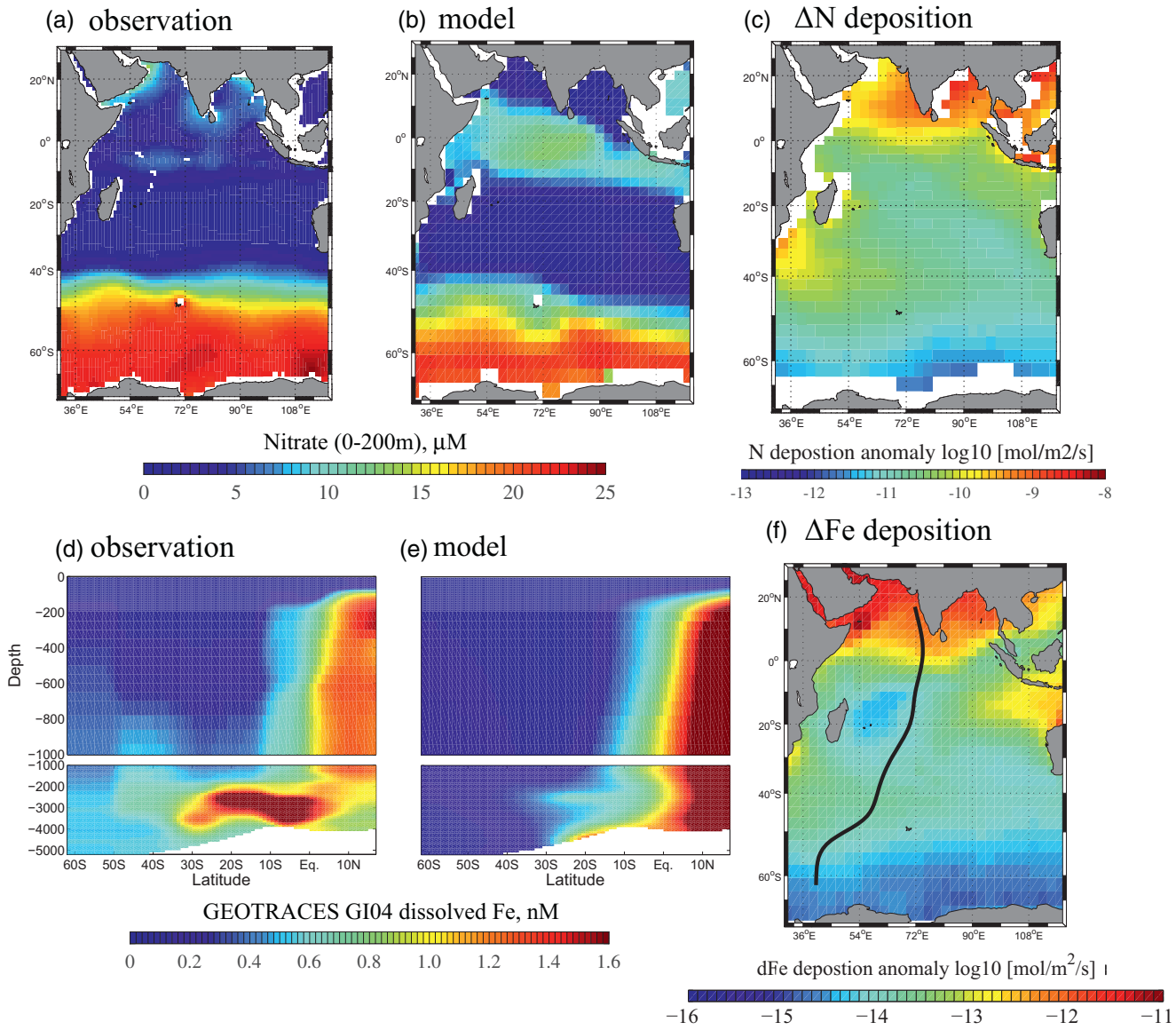


**Figure 1.** Upper panel (a): World Ocean Atlas Annual Mean $NO_3^-$ averaged over the top 200 m, (b): Mean modeled $NO_3^-$ averaged over the top 200 m ocean—results from the *Ind* run, Lower panel (c): Atmospheric deposition anomaly (*Ind* run–*PreIn* run) of fixed N into the surface of the Indian Ocean used in this study, (d): Observed dFe concentration from the GEOTRACES program along the Indian Ocean GI04 transect, (e): dFe concentration—results from the *Ind* run—along the Indian Ocean GI04 transect. Observational and model dFe were interpolated into the same coordinate using objective mapping, and (f): Atmospheric deposition anomaly (*Ind* run–*PreIn* run) of dFe into the surface of the Indian Ocean. The black line indicates the track of GEOTRACES GI04 cruise in the Indian Ocean. Model results are from the final year of a 1000-year model run, which are at the quasisteady state.

model is missing important nutrient sources and tend to underestimate the biological productivity near the coasts and in the Southern Ocean. In addition, the NPP biases might be due to the model underestimation of the dFe concentration. Nevertheless, our model captured the general pattern of the observed NPP in the Indian Ocean. Since the NPP is an important indicator of the ocean organic carbon pumps, it is encouraging that our model started representing some features despite its low spatial resolution. However, it should be noted that the NPP value can vary by up to five folds between different algorithms used to produce the satellite-based product (Behrenfeld & Falkowski, 1997b). Specifically, the VGPM algorithm used in this study tends to have much lower NPP in the lower latitudes and much higher NPP in the Subantarctic.

Finally, we calculated the correlation coefficients, root mean square errors (RMSEs), and standard deviations between the model fields of salinity, temperature, and nutrients and available observations. Data for

$NO_3$−, $PO_4^{3-}$, salinity, and temperature are from the World Ocean Atlas 2018 (Garcia et al., 2019) and were interpolated to the model grid. The results were plotted in a series of Taylor diagrams, which are shown in Figure S2 of the supporting information. These Taylor diagrams confirm that our model captures the temperature, salinity, and nutrients distributions in the Indian Ocean reasonably well. The correlation coefficients between observed and model fields for temperature and salinity are >0.9, while these values for macronutrients fields are >0.8. More important, these figures show that the *Ind* model run with a complex Fe scheme is better in reproducing observations than the *simpleFe* run, even though both runs were forced by the same ocean circulation and atmospheric deposition forcings. In particular, the correlation coefficients and RMSE values for all nutrient fields are better for the *Ind* run than the *simpleFe* run, especially for the dFe field. From the *simpleFe* to the *Ind* model runs, the correlation coefficient for dFe switches from a negative value to a value of 0.7, the RMSE decreases from 0.6 to ∼0.4, and the standard deviation gets much closer to that of observations. This result indicates the importance of incorporating a more realistic Fe scheme in the ocean biogeochemistry model.

### 3.2. Sensitivity Experiments

The increase in the atmospheric deposition of fixed N and dFe into the Indian Ocean is shown in Figures 1c and 1f. A large increase in the dFe deposition occurred in the coastal regions of the northern Indian Ocean and north of Australia, while it moderately increased over the equatorial and southern regions. Integrating over the Indian Ocean (30°E–110°E, 80°S–30°N), the dFe flux increased from 38.78 to 87.78 mol/s, more than doubling the preindustrial deposition. N deposition exhibited a similar spatial pattern to dFe. Again integrating over the Indian Ocean, the fixed N flux increased from $6.3 \times 10^3$ to $1.3 \times 10^4$ mol/s, approximately doubling from its preindustrial value.

The response of the Indian ocean biogeochemistry to an increased deposition of N and dFe is examined in the euphotic zone (0–100 m), where the phytoplankton activity is strongest. Comparing *PreIn* and *Ind* runs, the response of the dFe concentration for the upper 100 m ocean after 100 years of anthropogenic deposition was an increase of approximately 0.3 nM in the northern Indian Ocean, whereas the response was much weaker poleward of 20°S (Figure 2a). This pattern was generally similar to the atmospheric deposition of dFe where the northern Indian Ocean received more anthropogenic dFe deposition relative to the Southern Ocean by several orders of magnitude. In contrast, the response of the near-surface $NO_3^-$ (Figure 2b) was very different from the atmospheric deposition pattern. $NO_3^-$ concentration generally decreased in the Indian Ocean even though the ocean received more N from atmospheric deposition. In particular, the N decrease was significant in the subtropical region between 20° and 40°S. There was also a region of significant N decrease in the Bay of Bengal. This change in the upper 100 m $NO_3$− concentration implies that the biological N uptake was enhanced in many parts of the Indian Ocean.

Other macro nutrients (P and Si) also decreased with the same pattern (Figures 2c and 2d). The P decrease was widespread and more enhanced in the Bay of Bengal and in the subtropics between 20° and 40°S. The decline of macronutrients between 20° and 40°S suggests that the increased Fe and N atmospheric deposition altered the productivity there even though the anthropogenic deposition was relatively weak in these regions and dFe concentration was close to be depleted.

We showed the responses of diatom and coccolithophore in Figure 3 and of the other four phytoplankton species in Figure S2.

Diatom concentration increased significantly in the south of 40°S, in the Bay of Bengal, and in the southeastern tropics, which are close to the regions of decrease in N, P, and Si (Figure 2).

In contrast, diatom concentrations weakened in the southern part of the Arabian Sea and slightly decreased along 40°S, close to regions having an increase in the coccolithophore (Figure 3b) and picoplankton (small phytoplankton) concentrations (Figure S2b). These changes indicate that diatom were out-competed in these regions by coccolithophore and picoplankton. One explanation for these changes is that diatom have a faster maximum growth rate but requires a higher P concentration relative to coccolithophore and picoplankton (Riegman et al., 2000). Thus, the decrease in P supply along 40°S and in the southern part of the

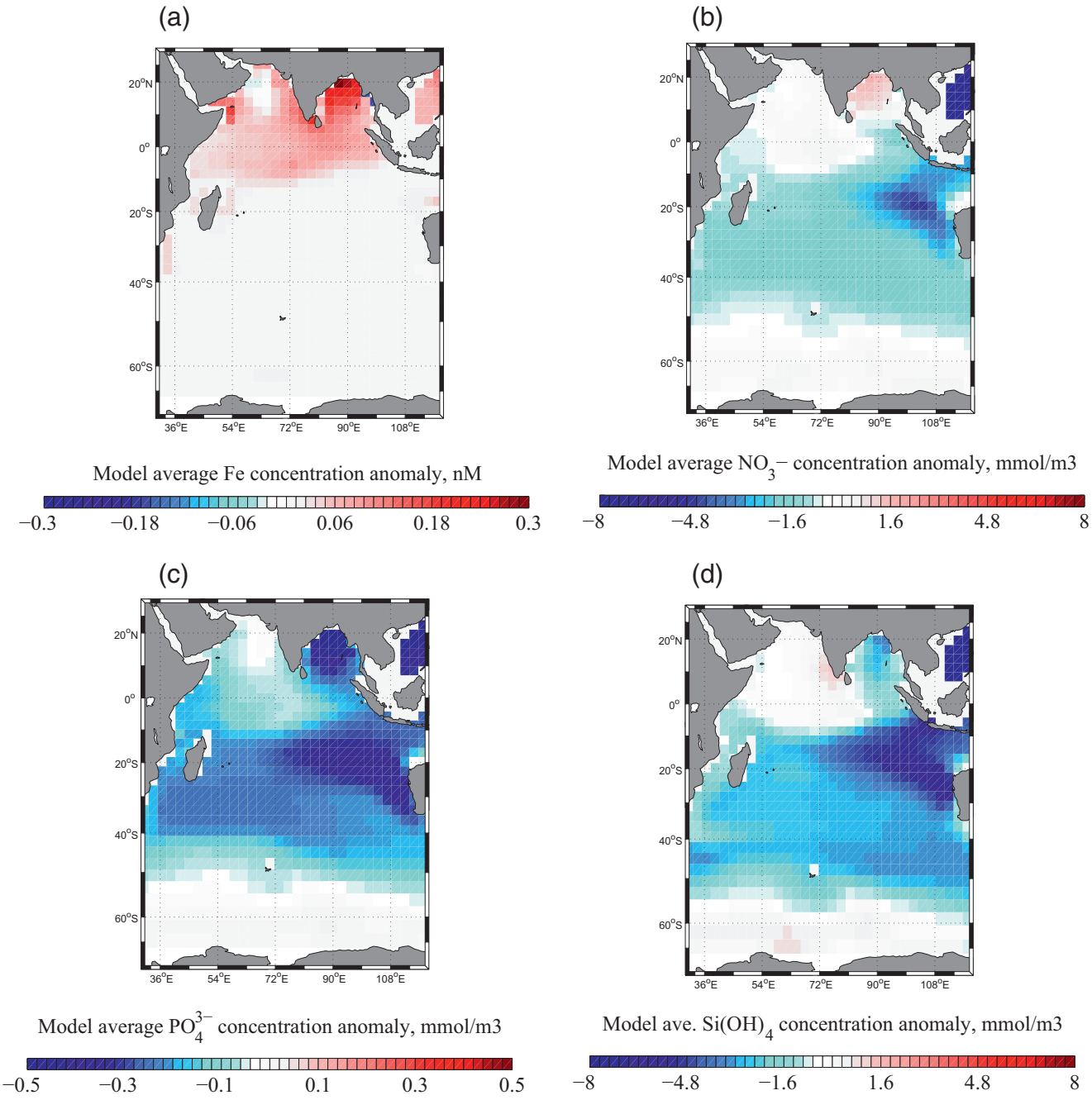


**Figure 2.** Model (*Ind* run) concentration anomaly relative to the *PreIn* run averaged from 0 to 100 m in the Indian Ocean for (a) dFe, (b) nitrate ($NO_3^-$), (c) phosphate ($PO_4^{3-}$), and (d) silicate ($SiO_2$) after 100 years of being forced under the anthropogenic N and Fe depositions. The responses are averaged over the last 10 years.

Arabian Sea caused diatom to be less competitive and helped coccolithophore and picoplankton become more dominant (Figure S8). In addition, diatom poleward of 40°S were relieved from Fe limitation and consumed more Si, therefore decreasing the Si transport equatorward and making diatom become Si-limited in the low latitudes (Figure S8). In the Bay of Bengal, the increased dFe deposition stimulated the growth of nitrogen-fixer diazotrophs (Figure S2). This stimulation of diazotrophs can alter the nitrogen cycle in the Bay of Bengal, but the $NO_3$− concentration change in this region seems to be relatively small (Figure 2). This relatively small change is probably due to compensations between different processes of the complex

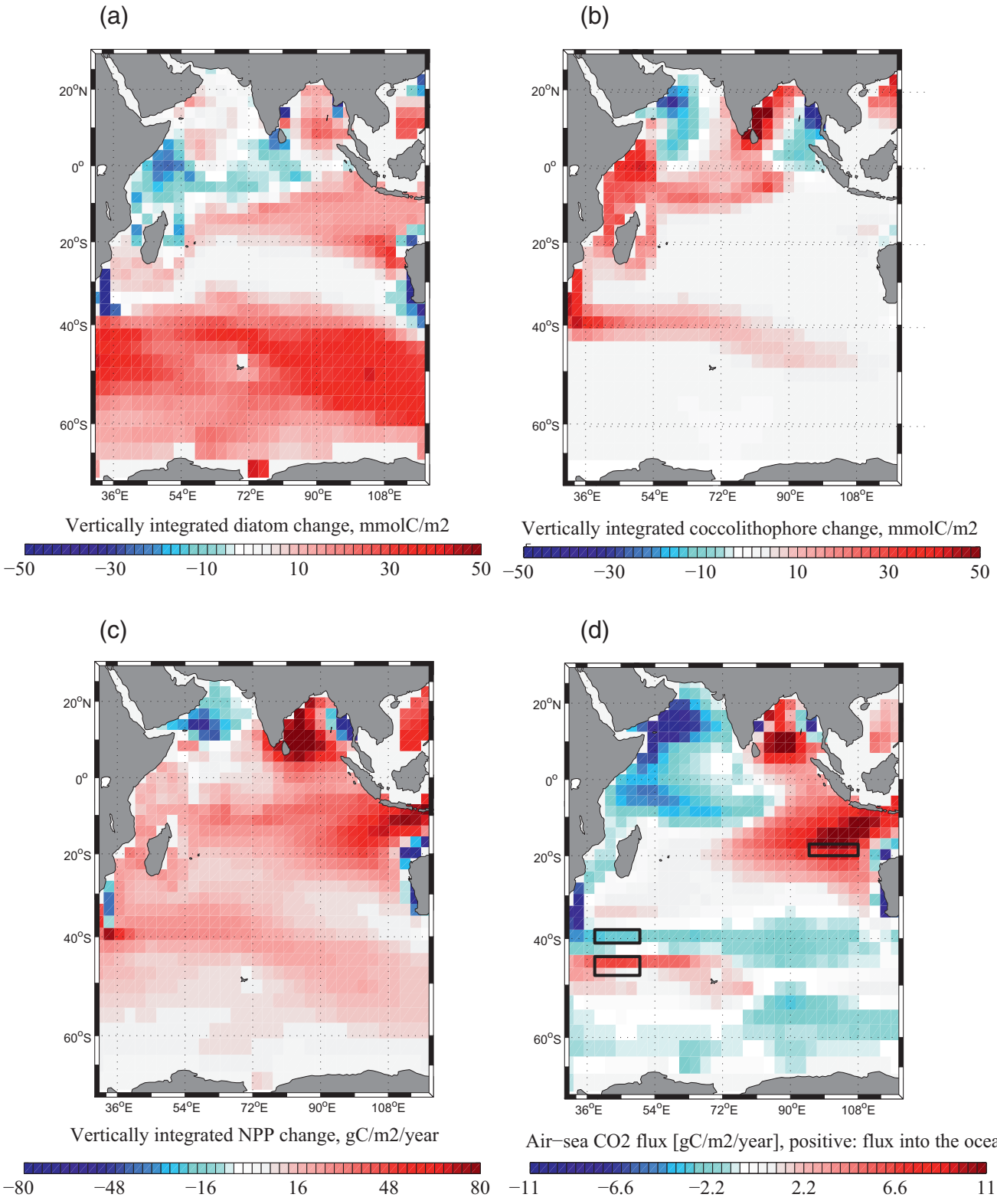


**Figure 3.** The vertically integrated anomaly between the *Ind* and the *PreIn* runs for (a) diatom concentration, (b) coccolithophore concentration, (c) primary production, and (d) air-sea $CO_2$ flux after 100 years of being forced under the anthropogenic N and Fe depositions. All phytoplankton biomass is measured in the unit of P in the model, which is converted to the unit of C using the ratio of 106:1. The air-sea $CO_2$ flux is positive into the ocean. The three black boxes shown in (d) are three regions where we will further analyze the evolution of changes in the phytoplankton community and air-sea $CO_2$ flux during the first 100 years after being forced by anthropogenic deposition. The responses are averaged over the last 10 years.

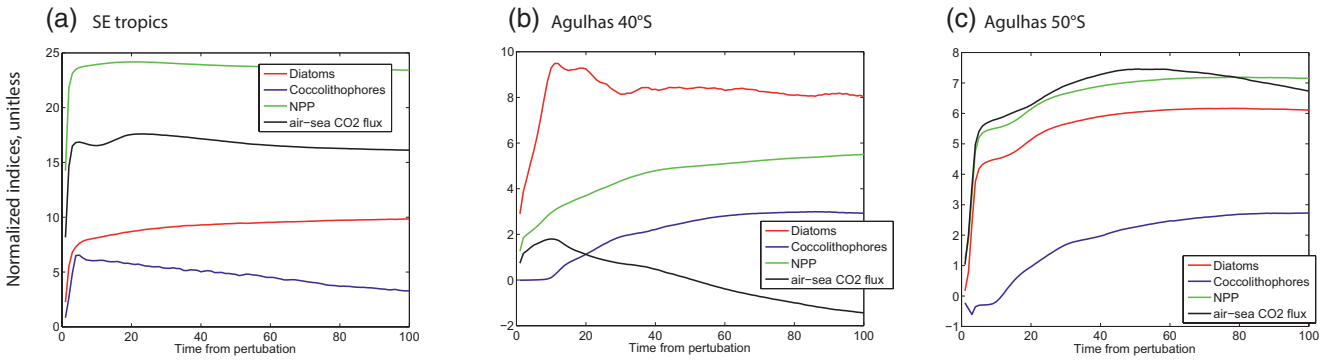


**Figure 4.** (a) The changes in the concentration of diatom (red lines), coccolithophore (blue lines), NPP (green lines), and the air-sea $CO_2$ flux (black lines) summed over the regions defined in Figure 3. (a) The southeastern (SE) tropics, (b) the Agulhas 40°S, (c) the Agulhas 50°S. All the changes in phytoplankton biomass and carbon uptake were normalized by dividing the change in each quantity by its standard deviation.

N cycle (Deutsch et al., 2007). In the northern Arabian Sea, diazotrophs concentration decreased together with coccolithophore and picoplankton due to a more intense P limitation in this region.

The competition between diatom and coccolithophore in the southern part of the Arabian Sea and along 40°S caused a shift in the biological carbon pump in these regions from organic to calcium carbonate pumps. An increase in coccolithophore and decrease in diatom decreased the surface alkalinity relative to dissolved inorganic carbon. Production of calcium carbonate shells consumed bicarbonate and carbonate ions, leading to a decrease in alkalinity. In turn, the decrease in surface alkalinity increased the ocean $CO_2$ and decreased the ocean buffer capacity. Consequently, it decreased the rate of ocean $CO_2$ uptake along 40°S and in the Arabian Sea (Figure 3d). This is somewhat counter-intuitive because the primary productivity indeed increased along 40°S and in the Southern Arabian sea under the modern atmospheric deposition. However, the intensified carbonate pump led to a decrease in the regional ocean carbon uptake. In contrast, the increase in diatom and picophytoplankton productivity along 50°S, the Bay of Bengal, and the southeastern tropical Indian Ocean contributed to a stronger organic carbon pump. In the Bay of Bengal, diazotrophs also increased. This increase in organic carbon pump outweighed the impact of coccolithophore and enhanced the ocean $CO_2$ uptake (Figure 3d). In the northern Arabian Sea, the organic carbon pump weakened because of the decrease in almost all phytoplankton species, which decreased the ocean $CO_2$ uptake. This region is one of the few regions in the Indian Ocean that showed a decrease in NPP under the impact of anthropogenic atmospheric nutrient deposition. In the Southern Ocean south of 50°S, the ocean $CO_2$ uptake also decreased, but through a different mechanism. In this region, a strong vertical mixing (Figure S12) brought the subsurface waters, which was loaded with more biological carbon due to an increase in NPP, to the surface, thereby causing the outgassing of $CO_2$. The map of vertical velocities at 100 m also shows that the ocean $CO_2$ uptake in regions of downwelling were most susceptible to changes in local community composition (along 40°S and in the southeastern tropics), while the ocean $CO_2$ uptake in regions of upwelling can be impacted by remote changes. In general, the competition between different phytoplankton species led to opposite responses in the regional ocean $CO_2$ uptake, despite an increase in the NPP almost everywhere.

We further analyzed the evolution of changes in the phytoplankton community and air-sea $CO_2$ flux during the first 100 years after being forced by anthropogenic deposition (Figure 4) in three regions shown in Figure 3d. These three regions include the southeastern tropics (SE tropics) and the regions along 40°S and 50°S in the south western Indian Ocean, close to the Agulhas current (Agulhas 40°S and Agulhas 50°S). In particular, we examined the evolution of changes during the first 100 years for diatom (red lines) and coccolithophore (blue lines) concentrations, NPP (green lines), and air-sea $CO_2$ flux (black lines). These three regions showed a contrasting response in the ocean $CO_2$ uptake flux even though their NPP all increased significantly after 100 years of being forced under the modern atmospheric deposition.

All the anomalies shown in Figure 4 were normalized (divided by the standard deviation) to facilitate the comparison between different quantities. In the SE tropics Figure 4a, diatom and coccolithophore concentrations both rapidly increased during the first 10 years under the anthropogenic deposition, which led to

an increase in the regional NPP and ocean $CO_2$ uptake. However, coccolithophore steadily decreased after this initial increase, whereas diatom kept growing. In this region, the effect of diatom increase dominated, leading to an increase in the NPP and the ocean $CO_2$ uptake after 100 years.

In contrast, coccolithophore in the Agulhas 40°S steadily increased over the 100-year time-frame, while diatom significantly enhanced during the first 10 years, then slightly decreased and stayed relative stable after 20 years Figure 4b. The increase in coccolithophore started dominating after around 20 years, which caused a decreasing trend of the air-sea $CO_2$ flux despite a continued increase in the NPP. After ∼50 years, the air-sea $CO_2$ flux changed its sign and this region became a source of carbon to the atmosphere.

The centennial evolution of phytoplankton community in the Agulhas 50°S is different than the other two regions Figure 4c. Both diatom and coccolithophore increased significantly, thus enhancing the primary production. The impact of enhanced diatom growth dominated in this region, which led to an increase in the ocean carbon uptake. In summary, our analysis here further demonstrated the compensation between the effects of growing diatom and coccolithophore, which controls the organic and calcium carbonate carbon pumps, ultimately determining the air-sea $CO_2$ flux.

The comparison between *PreIn*, *IndFe*, and *IndN* runs suggested that responses of the Indian Ocean ecosystems to anthropogenic depositions are mostly caused by the increase in dFe deposition (Figures S4–S7). The ocean responses from the *IndFe* run (Figures S4 and S5) look almost identical to the results of the *Ind* run. In contrast, results from the *IndN* run show negligible changes in the nutrient and phytoplankton fields (Figures S6 and S7), except for a slight increase in the surface concentrations of $NO_3-$ and $Si(OH)_4$. Results from *SimpleFe* run show that without proper representation for the internal Fe cycling scheme (ligand distribution and reversible scavenging process), the model dFe field in the Indian Ocean can be significantly biased (Figure S9). In this run, the surface dFe concentration is too high under the dust plume, and the deep dFe concentration is too uniformly high throughout the region. Biases in the Fe field can propagate and significantly alter the responses of the ocean ecosystem to human perturbations (Figures S10 and S11). In particular, the increase in surface dFe concentration spreads further to the Southern Ocean, but the responses from other nutrients, phytoplankton, primary production, and ocean carbon uptake are significantly reduced. This reduction in the ecosystem response is because the *SimpleFe* run tends to overestimate the dFe concentration in the Indian Ocean, especially in the southern part of the basin, therefore underestimating the Fe limitation of phytoplankton. Nevertheless, there are still features in the Southern Ocean and southeastern tropics demonstrating the competition between diatom and coccolithophore and its compensating effect on the ocean carbon uptake as seen in the *Ind* run.

## 4. Discussion and Conclusion

Human activities have heavily perturbed atmospheric deposition of dFe and N into the ocean since the start of the industrial era (Mahowald et al., 2009, 2017). This has a crucial consequence to the marine ecosystem in oligotrophic regions where phytoplankton is limited by N and HNLC regions where phytoplankton is limited by Fe. Earlier modeling studies estimated a modest response of the ocean primary production and air-sea $CO_2$ exchange to the anthropogenic nutrient deposition at the global scale, but also predicted striking responses of biogeochemical cycles at regional scales (Ito et al., 2016; Krishnamurthy et al., 2007, 2009; Somes et al., 2016). Specifically, Krishnamurthy et al. (2009) suggested that increasing dFe input stimulates marine nitrogen fixation in the subtropical North and South Pacific where Fe limitation of diazotrophs is relieved but decrease it in the Indian Ocean where diazotrophs become more P limited.

This study focused on the centennial response of the Indian Ocean ecosystem and carbon cycle to increased atmospheric nutrient inputs caused by the anthropogenic effects on aerosol deposition. We used a state-the-art ocean ecosystem and Fe cycling model, constrained by the new high-quality data of Fe from the GEOTRACES program (Mawji et al., 2015; Schlitzer et al., 2018). This new data set puts a much more stringent constraint on the representation of Fe cycling in the ocean biogeochemistry models, thereby improving our process-level understanding and quantification of key processes (Tagliabue et al., 2016, 2017). Our ocean model, when forced under the contemporary deposition (evaluated at year 2009), was able to reproduce many important features of the observed nutrient distributions and some important patterns of the NPP. Although the model still showed some biases, it captured major aspects of the subsurface dFe

**Table 1**
*The Export Production at 100 m (EP: PgC/Year), Air-Sea $CO_2$ flux (PgC/Year) (Positive Values Mean the Ocean Uptakes $CO_2$), and Diatom and Coccolithophore Biomass (TgC) Integrated Over the Indian Ocean (30°E–110°E, 80°S–30°N) (Results are Averaged Over the Last 10 Years After Being Forced by Different dFe and N Deposition Fluxes (mol/s) for 100 Years)*

| Model run | EP | $CO_2$ flux | Diatom | Cocco. | Fe dep. | N dep. |
|---|---|---|---|---|---|---|
| PreIn | 1.43 | 0.282 | 44.67 | 9.61 | 38.78 | $6.3 \times 10^3$ |
| Ind | 1.73 | 0.286 | 50.42 | 12.81 | 87.78 | $1.3 \times 10^4$ |
| IndFe | 1.72 | 0.288 | 50.46 | 12.69 | 87.78 | $6.3 \times 10^3$ |
| IndN | 1.44 | 0.288 | 45.66 | 8.67 | 38.78 | $1.3 \times 10^4$ |

pattern along the Indian Ocean GI04 transect remarkably well. Model experiments were designed to examine the centennial impacts of anthropogenic N and dFe deposition, separated from the other anthropogenic and natural drivers, such that we can clearly understand the mechanisms at play at a timescale that is relevant for human activities and policies. Of course, several different types of perturbations affect marine ecosystems and their biogeochemistry since the industrial revolution, including ocean warming, ocean circulation changes, riverine nutrient input, and acidification due to the uptake of fossil fuel $CO_2$. Among these perturbations, the anthropogenic nutrient input from rivers can provide a significant amount of N and P to the open ocean (Sharples et al., 2017). Thus, if this input were included in the model, the phytoplankton community in the northern Indian Ocean could be relieved of P limitation, and therefore the ocean primary production could be significantly enhanced. Nevertheless, a comprehensive analysis of the realistic, transient ecosystem changes is beyond the scope of this paper. Even in this idealized experiment, the response of ecosystems and the carbon cycle was complex and exhibited unique spatial patterns.

Even though both the atmospheric fluxes of N and dFe into the Indian Ocean doubled their values since the industrial revolution due to anthropogenic effects, the ocean ecosystem responses were mostly caused by the increase in dFe deposition alone. Because of this significant increase in dFe deposition, phytoplankton growth was enhanced when they were relieved from Fe limitation. Specifically, summing up over the whole basin, diatom biomass increased by 12% and coccolithophore increased by 33% (Table 1). As a result, the export production at 100 m summed up over the whole basin increased ~21%, (see Table 1). However, the ocean $CO_2$ uptake only slightly increased by 1% if integrated over the Indian Ocean. This slight increase in the ocean $CO_2$ uptake despite the significant increase in the NPP can be explained by analyzing changes in the ocean $CO_2$ uptake pattern and phytoplankton community structure, which did not respond uniformly under the anthropogenic deposition. In particular, productivity and carbon uptake both intensified along 50°S, in the southeastern tropics, and in the Bay of Bengal. These changes were influenced by the increasing diatom, and picophytoplankton productions and a stronger organic carbon pump. In contrast, the northern Arabian Sea exhibited decreased productivity and a weaker carbon uptake due to the intensification of P limitation. An increase in coccolithophore production along 40°S and in the southern Arabian Sea led to a stronger calcium carbonate pump at the expense of diatom productivity. This caused the ocean carbon uptake to weaken even though the local primary productivity increased. It should be noted that our model underestimated the vertically integrated NPP relative to satellite-based observations, which could lead to biases in the air-sea $CO_2$ response. The biases in NPP is mostly in the mid-latitude and southern part of the Indian Ocean (south of 20°S) where the current model's coarse resolution could not represent the coastal current systems and eddies adequately. Despite this caveat, our results suggest that the regional pattern of responses in the NPP and ocean carbon uptake to anthropogenic forcings can be much more complicated than a uniform increase, which is due to competitions within the phytoplankton community. It is difficult to compare the results of our model with the long-term trend of observation-based air-sea $CO_2$ flux in the Indian Ocean and infer a single mechanism underlying the observed trend (Landschützer et al., 2016). First, the data for air-sea $CO_2$ flux are very sparse in the Indian and Southern Oceans. Thus, even if there are any trends in the pattern of observed-based air-sea $CO_2$ flux, it's hard to attribute this trend to a specific mechanism. In addition, the ENSO related pattern (EOF-2) of the air-sea $CO_2$ flux shown in Landschützer et al. (2016) has a structure similar to what we showed in Figure 3d. This similarity makes it difficult to separate the relative contribution of anthropogenic nutrient deposition to changes in the air-sea $CO_2$ flux from climate variability.

Moreover, we showed that without a realistic representation of the ocean Fe cycle, modeling results on the ocean responses to human perturbations can be significantly biased. Models that have a uniform, constant ligand class tend to overestimate the dFe ocean concentration, which in turn leads to a muted response of the phytoplankton community and ocean carbon uptake.

The Indian Ocean is an important region of the world ocean, containing a large volume of low $O_2$ water in the north where phytoplankton is limited by macronutrients (Stramma et al., 2010) and a HNLC region in

the southern sector where biological productivity is limited by Fe (Twining et al., 2019). This diverse and complex region is vulnerable to an increase in atmospheric inputs of N and dFe due to industrial activities (Baker et al., 2017; Duce et al., 2008; Mahowald et al., 2009). Our results suggested that anthropogenic aerosol inputs may moderately increase the basin-scale productivity over a centennial timescale but may cause significant changes in the regional patterns of productivity and the composition of the phytoplankton community. The latter change can alter the functioning of the biological carbon pump with nonnegligible impacts on the basin-scale patterns of carbon uptake. Previous studies have pointed to an increase in coccolithophore biomass under global warming and increasing $CO_2$ concentration with important consequences to the ocean calcification and global carbon cycle (Krumhardt et al., 2016, 2019; Krumhardt, Lovenduski, Iglesias-Rodriguez, et al., 2017; Krumhardt, Lovenduski, Long, et al., 2017). We further emphasized the crucial role of this calcifier phytoplankton due to its sensitivity to nutrient inputs. In conclusion, our results suggested a complicated and strong, regional sensitivity of the ecosystem and carbon fluxes in the Indian Ocean under the impact of anthropogenic pollution.

## Data Availability Statement

The model outputs, relevant data, and MATLAB scripts to reproduce the figures shown in this manuscript are stored at Zenodo (https://doi.org/10.5281/zenodo.3866205).

**Acknowledgments**
We acknowledge the GEOTRACES group for making the dissolved iron transect data publicly available in its website: http://www.egeotraces.orgWe thank Stephanie Dutkiewicz, Martial Taillefert, Pearse Buchanan, and an anonymous reviewer for providing helpful comments and suggestion. Anh L. D. Pham is grateful for the support by the ANR project CIGOEF (Grant number ANR-17-CE32-0008). Takamitsu Ito is thankful for the funding support by the National Science Foundation (Grant number 1744755, 1737188).

## References

Baker, A. R., Kanakidou, M., Altieri, K. E., Daskalakis, N., Okin, G. S., Myriokefalitakis, S., & Prospero, J. M. (2017). Observation- and model-based estimates of particulate dry nitrogen deposition to the oceans. *Atmospheric Chemistry and Physics*, *17*(13), 8189–8210. https://doi.org/10.5194/acp-17-8189-2017. Retrieved from https://www.atmos-chem-phys.net/17/8189/2017/

Behrenfeld, M. J., & Falkowski, P. G. (1997a). A consumer's guide to phytoplankton primary productivity models. *Limnology & Oceanography*, *42*(7), 1479–1491. https://doi.org/10.4319/lo.1997.42.7.1479

Behrenfeld, M. J., & Falkowski, P. G. (1997b). Photosynthetic rates derived from satellite-based chlorophyll concentration. *Limnology & Oceanography*, *42*(1), 1–20. https://doi.org/10.4319/lo.1997.42.1.0001

Boyd, P. W., Ibisanmi, E., Sander, S. G., Hunter, K. A., & Jackson, G. A. (2010). Remineralization of upper ocean particles: Implications for iron biogeochemistry. *Limnology & Oceanography*, *55*(3), 1271–1288. https://doi.org/10.4319/lo.2010.55.3.1271

Boyd, P. W., & Tagliabue, A. (2015). Using the l* concept to explore controls on the relationship between paired ligand and dissolved iron concentrations in the ocean. *Marine Chemistry*, *173*, 52–66. Retrieved from http://www.sciencedirect.com/science/article/pii/S0304420314002254. http://dx.doi.org/10.1016/j.marchem.2014.12.003

Chinni, V., Singh, S. K., Bhushan, R., Rengarajan, R., & Sarma, V. (2019). Spatial variability in dissolved iron concentrations in the marginal and open waters of the indian ocean. *Marine Chemistry*, *208*, 11–28. Retrieved from http://www.sciencedirect.com/science/article/pii/S0304420318300586. https://doi.org/10.1016/j.marchem.2018.11.007

Deutsch, C., Sarmiento, J. L., Sigman, D. M., Gruber, N., & Dunne, J. P. (2007). Spatial coupling of nitrogen inputs and losses in the ocean. *Nature*, *445*, 163. https://doi.org/10.1038/nature05392. Retrieved from https://www.nature.com/articles/nature05392#supplementary-information

Duce, R. A., LaRoche, J., Altieri, K., Arrigo, K. R., Baker, A. R., Capone, D. G., & Zamora, L. (2008). Impacts of atmospheric anthropogenic nitrogen on the open ocean. *Science*, *320*, 893–897. https://doi.org/10.1126/science.1150369. Retrieved from https://science.sciencemag.org/content/sci/320/5878/893.full.pdf

Dutkiewicz, S., Follows, M. J., & Bragg, J. G. (2009). Modeling the coupling of ocean ecology and biogeochemistry. *Global Biogeochemical Cycles*, *23*(4), GB4017. https://doi.org/10.1029/2008GB003405. Retrieved from https://agupubs.onlinelibrary.wiley.com/doi/abs/10.1029/2008GB003405

Dutkiewicz, S., Scott, J. R., & Follows, M. J. (2013). Winners and losers: Ecological and biogeochemical changes in a warming ocean. *Global Biogeochemical Cycles*, *27*(2), 463–477. https://doi.org/10.1002/gbc.20042. Retrieved from https://agupubs.onlinelibrary.wiley.com/doi/abs/10.1002/gbc.20042

Dutkiewicz, S., Ward, B. A., Monteiro, F., & Follows, M. J. (2012). Interconnection of nitrogen fixers and iron in the Pacific Ocean: Theory and numerical simulations. *Global Biogeochemical Cycles*, *26*(1), GB1012. https://doi.org/10.1029/2011GB004039. Retrieved from https://agupubs.onlinelibrary.wiley.com/doi/abs/10.1029/2011GB004039

Dutkiewicz, S., Ward, B. A., Scott, J. R., & Follows, M. J. (2014). Understanding predicted shifts in diazotroph biogeography using resource competition theory. *Biogeosciences*, *11*(19), 5445–5461. https://doi.org/10.5194/bg-11-5445-2014. Retrieved from http://www.biogeosciences.net/11/5445/2014/

Fitzsimmons, J. N., John, S. G., Marsay, C. M., Hoffman, C. L., Nicholas, S. L., Toner, B. M., et al. (2017). Iron persistence in a distal hydrothermal plume supported by dissolved-particulate exchange. *Nature Geoscience*, *10*, 195–201. https://doi.org/10.1038/ngeo2900. Retrieved from http://www.nature.com/ngeo/journal/vaop/ncurrent/abs/ngeo2900.html#supplementary-information

Garcia, H. E., Locarini, R., Boyer, T., Antono, J., Baranova, O., Zweng, M., et al. (2014). World ocean atlas 2013. In S. Levitus & A. Mishonov (Eds.), Dissolved oxygen, apparent oxygen utilization, and oxygen saturation (Technical Ed. 3, 3, p. 27). NOAA Atlas NESDIS 75.

Garcia, H. E., Weathers, K., Paver, C. R. C., Smolyar, I., Boyer, T., Locarini, M., et al. (2019). World ocean atlas 2018. In A. Mishonov (Ed.), *Dissolved inorganic nutrients (phosphate, nitrate and nitrate+nitrite, silicate)* (Technical Ed. 4, p. 35). NOAA Atlas NESDIS 84.

Geider, R. J., MacIntyre, H. L., & Kana, T. M. (1998). A dynamic regulatory model of phytoplanktonic acclimation to light, nutrients, and temperature. *Limnology & Oceanography*, *43*(4), 679–694. https://doi.org/10.4319/lo.1998.43.4.0679. Retrieved from https://aslopubs.onlinelibrary.wiley.com/doi/abs/10.4319/lo.1998.43.4.0679

Gent, P. R., & Mcwilliams, J. C. (1990). Isopycnal mixing in ocean circulation models. *Journal of Physical Oceanography*, *20*(1), 150–155. https://doi.org/10.1175/1520-0485(1990)020<0150:imiocm>2.0.co;2. Retrieved from https://journals.ametsoc.org/doi/abs/10.1175/1520-0485%281990%29020%3C0150%3AIMIOCM%3E2.0.CO%3B2

Guieu, C., Al Azhar, M., Aumont, O., Mahowald, N., Levy, M., Ethé, C., & Lachkar, Z. (2019). Major impact of dust deposition on the productivity of the Arabian Sea. *Geophysical Research Letters*, *46*(12), 6736–6744. https://doi.org/10.1029/2019gl082770. Retrieved from https://agupubs.onlinelibrary.wiley.com/doi/abs/10.1029/2019GL082770

Hickman, A. E., Dutkiewicz, S., Williams, R. G., & Follows, M. J. (2010). Modelling the effects of chromatic adaptation on phytoplankton community structure in the oligotrophic ocean. *Marine Ecology Progress Series*, *406*, 1–17. Retrieved from https://www.int-res.com/abstracts/meps/v406/p1-17/

Ito, T., Nenes, A., Johnson, M. S., Meskhidze, N., & Deutsch, C. (2016). Acceleration of oxygen decline in the tropical pacific over the past decades by aerosol pollutants. *Nature Geoscience*, *9*(6), 443–447. https://doi.org/10.1038/ngeo2717. Retrieved from http://www.nature.com/ngeo/journal/v9/n6/abs/ngeo2717.html#supplementary-information

Johnson, M. S., & Meskhidze, N. (2013). Atmospheric dissolved iron deposition to the global oceans: Effects of oxalate-promoted fe dissolution, photochemical redox cycling, and dust mineralogy. *Geoscientific Model Development*, *6*(4), 1137–1155. https://doi.org/10.5194/gmd-6-1137-2013. Retrieved from http://www.geosci-model-dev.net/6/1137/2013/

Kalnay, E., Kanamitsu, M., Kistler, R., Collins, W., Deaven, D., Gandin, L., & Joseph, D. (1996). The NCEP/NCAR 40-year reanalysis project. *Bulletin of the American Meteorological Society*, *77*(3), 437–472. https://doi.org/10.1175/1520-0477(1996)077<0437:TNYRP>2.0.CO;2

Krishnamurthy, A., Moore, J. K., Mahowald, N., Luo, C., Doney, S. C., Lindsay, K., & Zender, C. S. (2009). Impacts of increasing anthropogenic soluble iron and nitrogen deposition on ocean biogeochemistry. *Global Biogeochemical Cycles*, *23*(3), GB3016. https://doi.org/10.1029/2008gb003440. Retrieved from https://agupubs.onlinelibrary.wiley.com/doi/abs/10.1029/2008GB003440

Krishnamurthy, A., Moore, J. K., Zender, C. S., & Luo, C. (2007). Effects of atmospheric inorganic nitrogen deposition on ocean biogeochemistry. *Journal of Geophysical Research: Biogeosciences*, *112*(G2), G02019. https://doi.org/10.1029/2006jg000334. Retrieved from https://agupubs.onlinelibrary.wiley.com/doi/abs/10.1029/2006JG000334

Krumhardt, K. M., Lovenduski, N. S., Freeman, N. M., & Bates, N. R. (2016). Apparent increase in coccolithophore abundance in the subtropical north atlantic from 1990 to 2014. *Biogeosciences*, *13*(4), 1163–1177. https://doi.org/10.5194/bg-13-1163-2016. Retrieved from https://www.biogeosciences.net/13/1163/2016/

Krumhardt, K. M., Lovenduski, N. S., Iglesias-Rodriguez, M. D., & Kleypas, J. A. (2017). Coccolithophore growth and calcification in a changing ocean. *Progress in Oceanography*, *159*, 276–295. Retrieved from http://www.sciencedirect.com/science/article/pii/S0079661117302148 https://doi.org/10.1016/j.pocean.2017.10.007

Krumhardt, K. M., Lovenduski, N. S., Long, M. C., Levy, M., Lindsay, K., Moore, J. K., & Nissen, C. (2019). Coccolithophore growth and calcification in an acidified ocean: Insights from community earth system model simulations. *Journal of Advances in Modeling Earth Systems*, *11*(5), 1418–1437. https://doi.org/10.1029/2018ms001483. Retrieved from https://agupubs.onlinelibrary.wiley.com/doi/abs/10.1029/2018MS001483

Krumhardt, K. M., Lovenduski, N. S., Long, M. C., & Lindsay, K. (2017). Avoidable impacts of ocean warming on marine primary production: Insights from the cesm ensembles. *Global Biogeochemical Cycles*, *31*(1), 114–133. https://doi.org/10.1002/2016gb005528. Retrieved from https://agupubs.onlinelibrary.wiley.com/doi/abs/10.1002/2016GB005528

Landschützer, P., Gruber, N., & Bakker, D. C. E. (2016). Decadal variations and trends of the global ocean carbon sink. *Global Biogeochemical Cycles*, *30*(10), 1396–1417. Retrieved from https://agupubs.onlinelibrary.wiley.com/doi/abs/10.1002/2015GB005359. https://doi.org/10.1002/2015GB005359

Large, W. G., McWilliams, J. C., & Doney, S. C. (1994). Oceanic vertical mixing: A review and a model with a nonlocal boundary layer parameterization. *Reviews of Geophysics*, *32*(4), 363–403. https://doi.org/10.1029/94RG01872

Mahowald, N. M., Engelstaedter, S., Luo, C., Sealy, A., Artaxo, P., Benitez-Nelson, C., & Siefert, R. L. (2009). Atmospheric iron deposition: Global distribution, variability, and human perturbations. *Annual Review of Marine Science*, *1*(1), 245–278. https://doi.org/10.1146/annurev.marine.010908.163727. Retrieved from http://www.annualreviews.org/doi/abs/10.1146/annurev.marine.010908.163727

Mahowald, N. M., Scanza, R., Brahney, J., Goodale, C. L., Hess, P. G., Moore, J. K., & Neff, J. (2017). Aerosol deposition impacts on land and ocean carbon cycles. *Current Climate Change Reports*, *3*(1), 16–31. https://doi.org/10.1007/s40641-017-0056-z

Marshall, J., Adcroft, A., Hill, C., Perelman, L., & Heisey, C. (1997). A finite-volume, incompressible navier stokes model for studies of the ocean on parallel computers. *Journal of Geophysical Research*, *102*(C3), 5753–5766. https://doi.org/10.1029/96JC02775

Marshall, J., Hill, C., Perelman, L., & Adcroft, A. (1997). Hydrostatic, quasi-hydrostatic, and nonhydrostatic ocean modeling. *Journal of Geophysical Research*, *102*(C3), 5733–5752. https://doi.org/10.1029/96JC02776

Mawji, E., Schlitzer, R., Dodas, E. M., Abadie, C., Abouchami, W., Anderson, R. F., et al. (2015). The geotraces intermediate data product 2014. *Marine Chemistry*, *177*(Part 1), 1–8. Retrieved from http://www.sciencedirect.com/science/article/pii/S0304420315000997. http://dx.doi.org/10.1016/j.marchem.2015.04.005

Mishra, R. K., Naik, R. K., & Anil Kumar, N. (2015). Adaptations of phytoplankton in the indian ocean sector of the Southern Ocean during austral summer of 1998—2014. *Frontiers of Earth Science*, *9*(4), 742–752. https://doi.org/10.1007/s11707-015-0541-4

Moffett, J. W., Vedamati, J., Goepfert, T. J., Pratihary, A., Gauns, M., & Naqvi, S. W. A. (2015). Biogeochemistry of iron in the arabian sea. *Limnology & Oceanography*, *60*(5), 1671–1688. https://doi.org/10.1002/lno.10132. Retrieved from https://aslopubs.onlinelibrary.wiley.com/doi/abs/10.1002/lno.10132

Moore, C. M., Mills, M. M., Arrigo, K. R., Berman-Frank, I., Bopp, L., Boyd, P. W., et al. (2013). Processes and patterns of oceanic nutrient limitation. *Nature Geoscience*, *6*(9), 701–710. https://doi.org/10.1038/ngeo1765. Retrieved from http://www.nature.com/ngeo/journal/v6/n9/abs/ngeo1765.html#supplementary-information

Naik, R. K., George, J., Soares, M., Anilkumar, N., Mishra, R., Roy, R., et al. (2020). Observations of surface water phytoplankton community in the Indian Ocean: A transect from tropics to polar latitudes. *Deep Sea Research Part II: Topical Studies in Oceanography*, *178*, 104848. Retrieved from http://www.sciencedirect.com/science/article/pii/S0967064519300438. https://doi.org/10.1016/j.dsr2.2020.104848

Nishioka, J., Obata, H., & Tsumune, D. (2013). Evidence of an extensive spread of hydrothermal dissolved iron in the Indian Ocean. *Earth and Planetary Science Letters*, *361*, 26–33. Retrieved from http://www.sciencedirect.com/science/article/pii/S0012821X12006589. http://dx.doi.org/10.1016/j.epsl.2012.11.040

Pham, A. L. D., & Ito, T. (2018). Formation and maintenance of the geotraces subsurface-dissolved iron maxima in an ocean biogeochemistry model. *Global Biogeochemical Cycles*, *32*(6), 932–953. https://doi.org/10.1029/2017GB005852

Pham, A. L. D., & Ito, T. (2019). Ligand binding strength explains the distribution of iron in the north Atlantic Ocean. *Geophysical Research Letters*, *46*(13), 7500–7508. https://doi.org/10.1029/2019gl083319. Retrieved from https://agupubs.onlinelibrary.wiley.com/doi/abs/10.1029/2019GL083319

Riegman, R., Stolte, W., Noordeloos, A. A. M., & Slezak, D. (2000). Nutrient uptake and alkaline phosphatase (EC 3:1:3:1) activity of Emiliania huxleyi (Prymnesiophyceae) during growth under n and p limitation in continuous cultures. *Journal of Phycology*, *36*(1), 87–96. https://doi.org/10.1046/j.1529-8817.2000.99023.x

Roxy, M. K., Modi, A., Murtugudde, R., Valsala, V., Panickal, S., Prasanna Kumar, S., et al. (2016). A reduction in marine primary productivity driven by rapid warming over the tropical Indian Ocean. *Geophysical Research Letters*, *43*(2), 826–833. Retrieved from https://agupubs.onlinelibrary.wiley.com/doi/abs/10.1002/2015GL066979. https://doi.org/10.1002/2015GL066979

Schlitzer, R., Anderson, R. F., Dodas, E. M., Lohan, M., Geibert, W., Tagliabue, A., et al. (2018). The geotraces intermediate data product 2017. *Chemical Geology*, *493*, 210–223. Retrieved from http://www.sciencedirect.com/science/article/pii/S0009254118302961. https://doi.org/10.1016/j.chemgeo.2018.05.040

Sharples, J., Middelburg, J. J., Fennel, K., & Jickells, T. D. (2017). What proportion of riverine nutrients reaches the open ocean? *Global Biogeochemical Cycles*, *31*(1), 39–58. https://doi.org/10.1002/2016GB005483

Somes, C. J., Landolfi, A., Koeve, W., & Oschlies, A. (2016). Limited impact of atmospheric nitrogen deposition on marine productivity due to biogeochemical feedbacks in a global ocean model. *Geophysical Research Letters*, *43*(9), 4500–4509. https://doi.org/10.1002/2016GL068335

Stramma, L., Schmidtko, S., Levin, L. A., & Johnson, G. C. (2010). Ocean oxygen minima expansions and their biological impacts. *Deep Sea Research Part I: Oceanographic Research Papers*, *57*(4), 587–595. Retrieved from http://www.sciencedirect.com/science/article/pii/S0967063710000294. https://doi.org/10.1016/j.dsr.2010.01.005

Tagliabue, A., Aumont, O., DeAth, R., Dunne, J. P., Dutkiewicz, S., Galbraith, E., et al. (2016). How well do global ocean biogeochemistry models simulate dissolved iron distributions? *Global Biogeochemical Cycles*, *30*(2), 149–174. https://doi.org/10.1002/2015GB005289

Tagliabue, A., Bowie, A. R., Boyd, P. W., Buck, K. N., Johnson, K. S., & Saito, M. A. (2017). The integral role of iron in ocean biogeochemistry. *Nature*, *543*(7643), 51–59. https://doi.org/10.1038/nature21058

Tripathy, S. C., Sabu, P., Patra, S., Naik, R. K., Sarkar, A., Venkataramana, V., & Sudarsanarao, P. (2020). Biophysical control on variability in phytoplankton production and composition in the south-western tropical Indian Ocean during monsoon 2014. *Frontiers in Marine Science*, *7*, 515. https://doi.org/10.3389/fmars.2020.00515. Retrieved from https://www.frontiersin.org/article/10.3389/fmars.2020.00515

Twining, B. S., Rauschenberg, S., Baer, S. E., Lomas, M. W., Martiny, A. C., & Antipova, O. (2019). A nutrient limitation mosaic in the eastern tropical Indian Ocean. *Deep Sea Research Part II: Topical Studies in Oceanography*, *166*, 125–140. Retrieved from http://www.sciencedirect.com/science/article/pii/S096706451830300X. https://doi.org/10.1016/j.dsr2.2019.05.001

Völker, C., & Tagliabue, A. (2015). Modeling organic iron-binding ligands in a three-dimensional biogeochemical ocean model. *Marine Chemistry*, *173*, 67–77. Retrieved from http://www.sciencedirect.com/science/article/pii/S0304420314002229. http://dx.doi.org/10.1016/j.marchem.2014.11.008

Wang, W.-L., Moore, J. K., Martiny, A. C., & Primeau, F. W. (2019). Convergent estimates of marine nitrogen fixation. *Nature*, *566*(7743), 205–211. https://doi.org/10.1038/s41586-019-0911-2

Ye, Y., & Völker, C. (2017). On the role of dust-deposited lithogenic particles for iron cycling in the tropical and subtropical Atlantic. *Global Biogeochemical Cycles*, *31*(10), 1543–1558. https://doi.org/10.1002/2017GB005663